Environmental Earth Sciences (2019) 78:84
https://doi.org/10.1007/s12665-019-8074-x

ORIGINAL ARTICLE

Alluvial aquifer thickness and bedrock structure delineation by electromagnetic methods in the highlands of Bolivia

Etzar Gómez[1,3] · Måns Larsson[2] · Torleif Dahlin[1] · Gerhard Barmen[1] · Jan-Erik Rosberg[1]

Received: 12 July 2017 / Accepted: 14 January 2019 / Published online: 28 January 2019
© The Author(s) 2019

Abstract

The porous aquifers in the area called Challapampa are the most important groundwater reservoirs that supply drinking water to Oruro city in the highlands of Bolivia. They consist of unconsolidated fluvial–lacustrine deposits, resting on a complex sedimentary bedrock and covered by a thin surficial clay layer. The settings of these geological units and the structures governing the flow patterns have barely been investigated, despite this reservoir having been utilized during the last 50 years. This study applied transient electromagnetic (TEM) soundings and electrical resistivity tomography (ERT) in the middle part of the alluvial fan of River Paria to investigate the thickness of the porous aquifer and detect the relief of the bedrock. Likewise, some results expressed as resistivity models indicate the possible existence of geological structures below the unconsolidated sediments. The average depth of investigation reached in this study is between 200 and 250 m below the surface, for both the applied methods. The geological structures inferred have similar directions as the major faults in the vicinity, from southeast to northwest, which in turn are assumed as part of fractured aquifers underlying the porous aquifers. The geo-electrical techniques were successfully tested in the study area and the resistivity models from TEM complement very well those obtained from ERT. Therefore, extended investigations using the same techniques would help to develop a more complete description of the hydrogeological settings of the aquifer system.

Keywords Transient electromagnetic · Resistivity · Hydrogeology · Bolivia

Introduction

In the semi-arid Bolivian Altiplano, aquifers are the most important source of water, since rivers and lakes have been drying out in the recent years because of the climate change. The aquifer system in the area called Challapampa, close to Oruro city, supplies water for consumption to about 300,000 inhabitants, besides being used for agriculture, mining and industrial purposes. This reservoir requires a management plan to assure its sustainability in the future. However, important characteristics like delimitation, geometry, classification of aquifers, estimation of storage volumes and recharge processes are not fully understood yet. To provide the information and data required to build up a complete description of the aquifer system, long-term hydrogeological investigations are needed. Geophysical methods have proven to be efficient and inexpensive tools in obtaining fast information about the distribution of physical properties in the subsurface. They also have proven to be efficient ways to investigate features such as saline water interface, depth and thickness of geological units and depth to water table (Auken

✉ Etzar Gómez
etzar.gomez@tg.lth.se

Måns Larsson
mablarsson@gmail.com

Torleif Dahlin
torleif.dahlin@tg.lth.se

Gerhard Barmen
gerhard.barmen@tg.lth.se

Jan-Erik Rosberg
jan-erik.rosberg@tg.lth.se

[1] Engineering Geology, Lund University, Box 118, 221 00 Lund, Sweden

[2] Department of Geology, Lund University, Box 118, 221 00 Lund, Sweden

[3] Institute of Hydraulic and Hydrology, San Andres Major University, La Paz, Bolivia

et al. 2003; Corriols et al. 2009; Gonzales et al. 2016; Guérin et al. 2001; Nabighian 1991).

There are just a few geophysical studies conducted in the Altiplano. Guérin et al. (2001) performed 100 time-domain electromagnetic (EM) soundings to identify saline groundwater in sediments in a big area in the Central Altiplano (1750 km^2). That study mentions the existence of large shallow conductive layers and brines limiting a good deep resolution using direct current (DC) methods. Other studies in different environments, demonstrated the good correlation between EM and DC methods (Boiero et al. 2010; Metwaly et al. 2010). The present study aims to combine TEM and ERT methods to describe an area where the water is supposed to be relatively fresh (low salinity), despite the proximity of some hot springs to the east with more saline water.

Information obtained from technical reports (not published) including DC measurements and drilling protocols in sites nearby the present study area, show the characteristics of the first 100 m below the soil surface, at this depth the bottom of the porous aquifers was not reached yet. This study aims to investigate the thickness of the unconsolidated sediments and structural features below those sediments, in the central and southeastern parts of the alluvial fan of River Paria (Fig. 1). The TEM method, the most relevant in this study, was selected because its proven good resolution in depth and its simplicity to arrange the equipment in the field. The results of the study intend to improve the knowledge about the geometry of the Challamapa aquifer system by clarifying the shape of the bedrock, estimating the thickness of the alluvial sediments and for evaluating the applicability of electromagnetic methods to map the entire aquifer in the future.

Study area

The Challapampa aquifer system belongs to the Poopo enclosed basin, located to the west side of the Cordillera Oriental (eastern mountain range of the Andes), where the highest peaks reach 4600 m above sea level (masl) and the

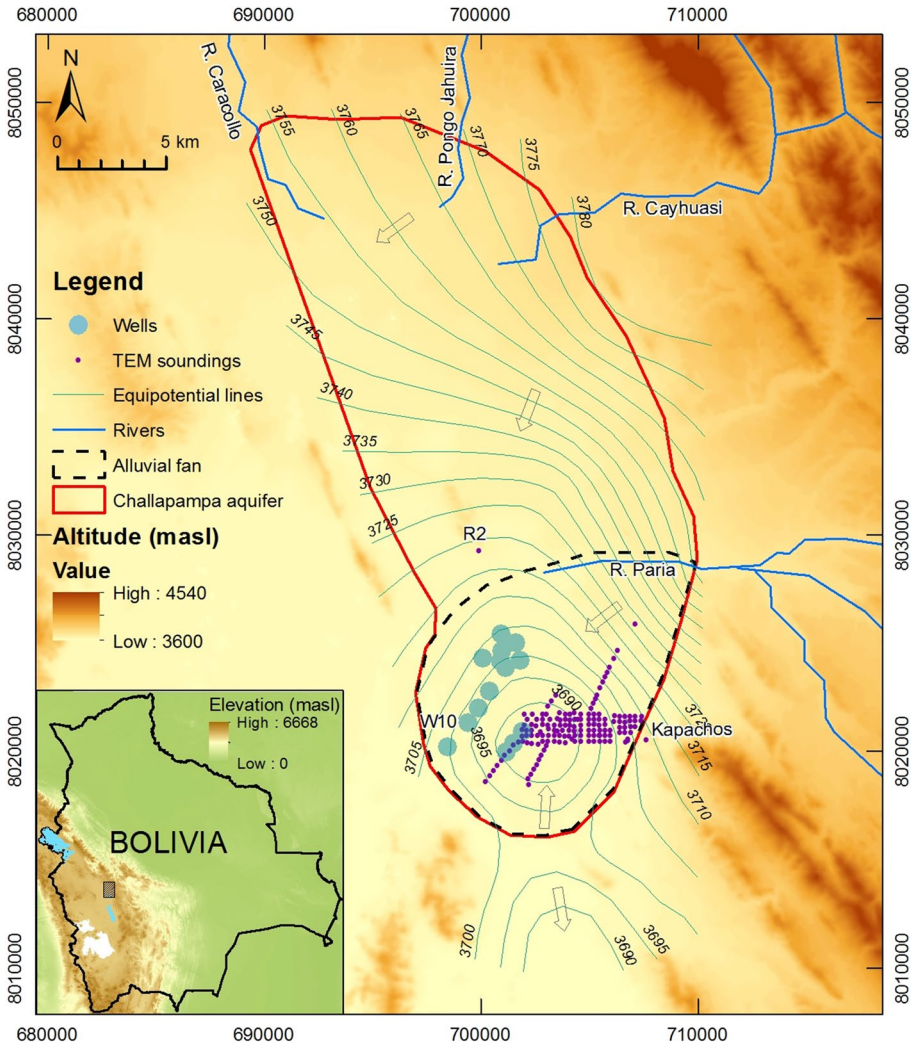

Fig. 1 Location of the Challapampa aquifer system in the Central Bolivian Altiplano. Part of it has been investigated applying TEM soundings. Arrows refer to the regional flow in the porous aquifers, within the first 100–160 m below the soil surface. Modified from GITEC and COBODES (2014); Swedish Geological (1996)

lowest and planar land is at 3700 masl (Fig. 1). In the Cordillera Oriental, the direction of the ridges is from northwest to southeast, which also defines the surrounding landscape and the bedrock relief below the porous aquifers.

The climate in the area is semi-arid, with scarce to non-existing vegetation. The average temperature is about 10 °C. Regarding precipitation, there is a big difference between summer and winter; about 80% of the mean annual 350 mm occurs from December to March (summer). In addition, the annual potential evaporation was estimated to be 1800 mm (SENAMHI 2015), evidencing the aridity of the region. During summer, intense precipitations create floods in the plateau, but the water is quickly evaporated leaving salt in the clayey soils. The land around the study area is mainly used for small-scale agriculture during the rainy season. Sporadic crops can be seen during the rest of the year in sites nearby the few wells used for irrigation in the vicinity. The alluvial fan of River Paria hosts a well field which abstracts water continuously, at a rate of about 300 l/s (SELA 2017), to supply Oruro. This situation has been affecting the piezometric levels in the irrigation wells and created social conflicts due to the limited access to water.

The Challapampa aquifer system is a generic name to refer all the geological formations yielding water in the region. The porous aquifers in the first ~ 100 m below the surface (mbs) are the main groundwater reservoirs near Oruro, characterized by the variety of the existing geological formations and the complexity of settings. The geological formations in the region can be divided into consolidated (rock) and unconsolidated (sediments). Among the first unit of rocks, sedimentary and metamorphic types are the most common in the bedrock (in purple in Fig. 2); also, igneous rocks are present in some volcanic intrusions (in orange in Fig. 2). The unconsolidated unit comprises sediments originated by erosional and depositional processes (in yellow in Fig. 2).

The consolidated rocks around and beneath the study area have folds and faults with northwest–southeast direction. Three Silurian formations have been identified in the bedrock and mountains (in purple in Fig. 2) where sandstones and siltstones are common. These formations are, from the oldest to the youngest, Llallagua, Uncia and Catavi (Suarez Soruco 2000). The Uncia and Catavi formations are exposed nearby the study site and according to the geological information, Uncia's bedrock underlies the Quaternary sediments. The bedrock might be comprised of green shales with beds of green sandstones and siltstones (GEOBOL and Swedish Geological 1992). Banks et al. (2002) include in their study a bedrock contour map (red lines in Fig. 2), based on drilling logs and geophysical tests like seismic refraction and vertical electrical soundings (VES), which in turn correspond to other previous studies not found in the present investigation. The deepest contact between sediments and bedrock might be located at 3540 masl (~ 160 mbs). Volcanic igneous rocks from the Tertiary are also part of the consolidated geological units; they are the so-called Oruro complex and Escalera volcanics. The first one, close to Oruro city, holds valuable minerals like silver, lead and others (Patureau 2007; Ramos et al. 2011). The second one, to the east of the study area, comprises rhyodacitic and porphyritic lavas (GEOBOL and Swedish Geological 1992). This intrusion might have a strong influence on the regional geothermal activity.

When it comes to the unconsolidated geological units, alluvial Quaternary sediments are the most extensive covering the relief of the bedrock and shaping the flat terrains. The grains in these deposits are mainly comprised of quartz and other silicates. They are largely variable in terms of grain size as well; pebbles, gravels, sands, silts and clays are all chaotically arranged because of the overlapping depositional processes. The well-rounded shape of pebbles and gravels lead to infer that they were transported long distances from the surrounding mountains by strong fluvial and glacial events. The finest sediments might correspond to lacustrine depositions, such is the case of the surficial clay layer (Rigsby et al. 2005). Figure 3 shows an example of how these sediments are arranged in a pit, in the first ~ 12 mbs. The thickness of the unconsolidated sediments of the porous aquifer may be from tenths to hundreds of meters, and the thickness of the surficial clay layer may be from tenths of centimeters to a couple of meters.

The most productive aquifers are the fluvial–lacustrine sediments of diverse thicknesses and settings. A few drilling logs, VES and debris excavations constitute the main sources of stratigraphic information in the study area, where the high vertical and lateral variability between different types of sediments is standing out, as shown in Fig. 3.

Hydrogeology

The Challapampa aquifer system has been studied at some drilling sites to obtain information to extract as much water as possible. However, most of that information was never properly saved and reported, and just a few investigations are available, e.g., Larsson (2016). The rest is partially or completely lost. In the study area, the geometry of the aquifer system was proposed by Banks et al. (2002) based on VES, seismic refraction and drilling logs (Dames & Moore Norge 2000; SCIDE et al. 1996). Unfortunately, just part of the information about stratigraphy is available. There are some drilling protocols around the well field area describing the stratigraphy of the first 100 mbs. These descriptions refer to the content of gravel, sand and clay at different levels. The stratigraphy obtained from those drilling reports is punctual and representative of few meters around the boreholes and not applicable to

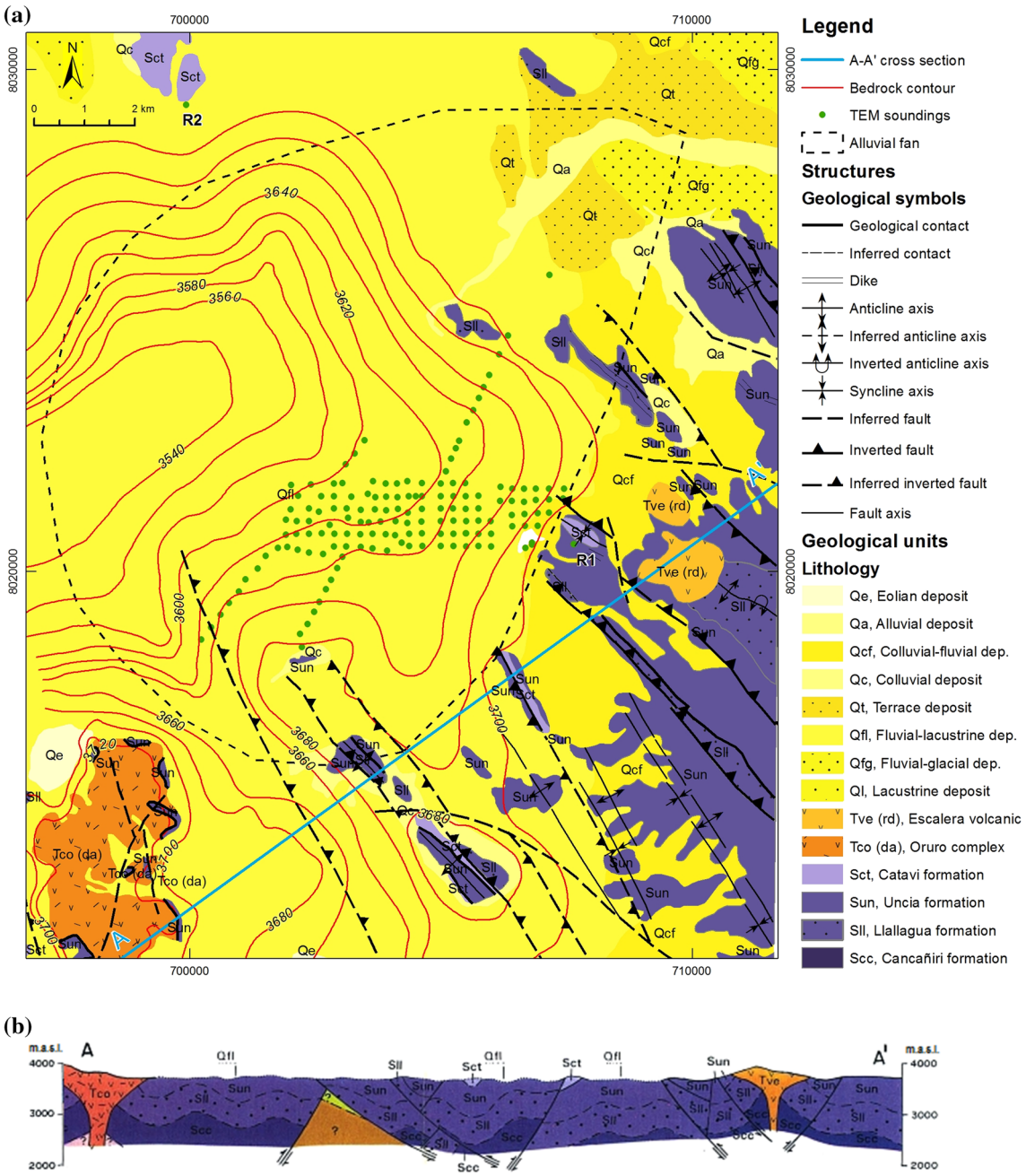

Fig. 2 **a** Geological map including bedrock contours and TEM soundings. **b** A–A′ cross-section. Quaternary sediments are not shown clearly due to the scale; the thickness of these units might be of a couple of meters in this section. Modified from Banks et al. (2002); GEOBOL and Swedish Geological (1992)

the rest of the alluvial fan, because of the high lateral and vertical variability in the arrangement of sediments. When it comes to the hydraulic conductivity, this variability ranges from 1.2E−5 to 5.8E−4 m/s in the unconsolidated sediments (Banks et al. 2002). Going deeper, the top, fractured and weathered part of the bedrock has values around $K = 1.0E{-}5$ m/s and for the consolidated sedimentary rock, it is about $K = 3.0E{-}8$ m/s (Dames & Moore Norge 2000).

According to the regional groundwater gradient (equipotential lines in Fig. 1), the flow seems to run from northeast to southwest in the porous aquifer. Precipitation in the mountains forms streams and rivers running towards the plane, which recharge the aquifers and then flows towards

Fig. 3 Excavation exposing about 12 mbs of sediments in the aquifer. This porous aquifer comprises gravel, sand and clay in different proportions according to the site and depth. However, clayey lenses are also interbedded in this geological package

the lowest site of the region, which might be the Lake Poopo, about 20 km south of the study area. However, the annual volumes of water extracted from the well field, about 9.5 million m^3 in 2016 (SELA 2017), have changed the natural flow direction and now it goes towards the central part of the alluvial fan, creating a cone of depression with a radius of influence of about 5 km around the well field (Banks et al. 2002).

In addition, hydrochemical and isotopic characteristics were used to propose four flow systems in the middle of the alluvial fan (Gómez et al. 2016), which are summarized in Table 1.

Geothermal activity also exists in the aquifer system, specifically to the east of the alluvial fan, in the site called Kapachos (Fig. 1). In this place, the water coming out from springs is hot and rich in total dissolved solids (high salinity), and the average temperature in the wells extracting from the porous aquifer is 15 °C and in the hot springs is ~ 50 °C. Salinity in terms of electrical conductivity (EC) in the wells extracting from the porous aquifers averages 1.0 mS/cm and in the hot springs is ~ 3.6 mS/cm. There are also boreholes, further away the present study site with thermal influence. For instance, in W10 in the wellfield (Fig. 1), the temperature is 30 °C and EC is 3.5 mS/cm. Flow paths and processes controlling the occurrence of the thermal water in the region remain unknown subjects out of the scope of this study.

Theory and methods

TEM is a point-based geophysical prospecting technique where a current flowing in a transmitter antenna generates a primary electromagnetic (EM) field. When that current is cut off, that primary EM field induces eddy currents flowing through the ground. Those eddy currents generate a secondary magnetic field detected by a receiver antenna. The receiver acquires time-dependent decaying voltage signals. During processing, those signals are transformed into electrical resistivity and vary as a function of the type of materials and how they are distributed in the ground (Christiansen et al. 2009; Reynolds 2011).

Water content and the type of water filling voids in the geological formations also determine the resistivity obtained by EM methods. Therefore, it is expected to find a distinction in terms of resistivity between saturated sediments

Table 1 Summary of flow systems and hydrogeological parameters in the Challapampa aquifer system (Banks et al. 2002; Dames & Moore Norge 2000; Gómez et al. 2016; Lizarazu et al. 1987)

Flow system depth (m)	Stratigraphic approach	Scheme	Hydraulic conductivity *K* (m/s)	Origin of water
0–20	Unconsolidated sediments	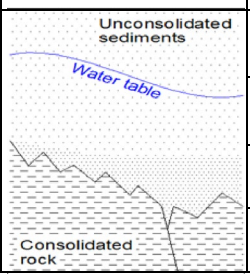	1.2E−5 to 5.8E−4	Direct infiltration
20–100	Unconsolidated sediments		1.2E−5 to 5.8E−4	Lateral recharge
100–400	Transition zone		1.0E−05*	Lateral recharge
> 400	Consolidated rock		3.0E−08	Unknown

**K* in the transition zone is similar to that in the unconsolidated sediments, because the tests to obtain that value were conducted in the fractured top part of the rock, according to Dames & Moore Norge (2000)

(main aquifers) and the bedrock (see Table 1) to establish the thickness of the saturated alluvial sediments.

The equipment used for the TEM measurements was an ABEM WalkTEM, connected to two batteries of 12 V transmitting dual moment electrical pulses: about 18 A during the high moment (HM) and about 2 A during the low moment (LM). An offset array was used during the tests, where a transmitter loop (50 × 50 m cable AWG #12) is placed next to the equipment. In the centre of the transmitter, the RC-5 receiver (0.5 × 0.5 m) is placed and the RC-200 receiver (10 × 10 m) is 50 m offset from the centre of the transmitter. Although both receivers were able to register both low and high moments, the RC-5 was used for measuring LM for better shallow resolution, and the RC-200 was used for measuring HM for better depth resolution.

Raw TEM data contains sorted information of HM, LM and noise in specific channels for both receivers. Before the inversion, HM channels corresponding to RC-5 and LM corresponding to RC-200 were disabled. Thus, the shallow part of the models was resolved with the RC-5 LM, and the deepest part with the RC-200 HM. Typical data curves, combining LM and HM, need to be trimmed in some specific parts like before intersecting with the noise curves, at the begging of HM and at the end of LM, where they are not overlapping each other within an acceptable displacement defined by error bars, and at any sudden fluctuation out of the shift of the curve.

After conducting measurements and conditioning the TEM data, the next step is to find a model that might reproduce the obtained data and be representative of the resistivity distribution in the test site. The process to find that model is called inverse numerical modeling, and for TEM it is based on curve matching aided by mathematical relationships and algorithms to solve an inverse scattering problem (Nabighian 1991). Data residual is an indicator of how small the differences are between the measured and the modeled data after a curve matching process. Two types of models are used to match the data curves; a layered model, where mean resistivity values correspond to a few layers, and a smooth model where gradual transitions in resistivity correspond to a fixed number of layers increasing in thickness by depth (Christiansen et al. 2009). The limit at which the resistivity structure of a model is reliable is the depth of investigation (DOI), below that limit the geological interpretations might not be true (Christiansen and Auken 2012). Likewise, the method has a minimum depth of resolution depending on the earliest acquisition times and shallow resistivity, which means that the top part of subsoil cannot be resolved with TEM (Spies 1989).

The inverse numerical modeling requires a lot of computing capacity for TEM, so accurate electronic components are also needed to get signals from a wide dynamic range. These issues became achievable during the last decades, making this technique relatively young in groundwater mapping applications (Christiansen et al. 2009). The TEM data were processed with SPIA (Aarhus GeoSoftware 2017a), which runs one-dimensional inversions of individual soundings. Finally, the creation of maps and cross-sections based on inverted TEM data was done with Aarhus Workbench (Aarhus GeoSoftware 2017b), which carry out interpolations with the closest one-dimensional models by the Kriging method.

Resistivity, as a physical property of geological formations was also evaluated with the ERT technique. In principle, the resistivity distribution in the ground corresponding to the same site from TEM and ERT is expected to be similar, although each method has its own characteristics making them sensitive to external factors (3-D effects, DOI, high conductive structures and others). For this study, resistivity obtained from TEM and ERT is assumed equally valid. A thorough analysis of the differences between both techniques is out of the limits of this study. Complementary ERT measurements were performed to obtain two-dimensional resistivity profiles. This technique is based on the DC methods in which the apparent resistivity of the subsoil is estimated by injecting electrical currents through a pair of electrodes and measuring the potential difference between another pair of electrodes. The geometry and type of arrangement of the electrodes determine the measured value of the apparent resistivity, as well as the intensity of current injected during the tests. Modern multi-electrode systems and automatized acquisition systems improved the efficiency of this technique (Dahlin 2001; Dahlin and Zhou 2006). The ERT measurements were conducted using two ABEM Terrameter LS equipment, each one together with four cables of 21 takeouts and stainless steel electrodes and connectors. The type of array selected for the measurements was multiple gradient due to its high speed data acquisition, good signal-to-noise ratio and high data density (Dahlin and Zhou 2006). The roll-along technique was used to reach distances of 2400 and 2000 m to the north and to the south, respectively. Likewise, the current injected was 500 and 200 mA in the northern and southern profiles. Similarly to the TEM data, the ERT data need to be processed and inverted. The process consists of minimizing the difference between the pseudo-section (apparent resistivity from the measurements) and the resultant resistivity from a synthetic model by refining this later in each iteration round. The final and refined synthetic model is assumed as the most likely representation of the resistivity distribution in the ground (Dahlin 2001; Loke et al. 2003). The software used to invert the ERT data in this study was Aarhus Workbench (Aarhus GeoSoftware 2017b), 2-D inversions were selected applying the L1-norm (robust constrain inversion), STD 1.3 for lateral constrain and STD 2.0 for vertical constrain to obtain the resistivity models.

Results and interpretations

The TEM data include 145 soundings, conducted from May to July 2016 in the study area. Those tests were distributed in a rectangular grid (about 6 km × 1.5 km) with ~ 250 m separation between soundings. Not all of them were uniformly separated, because potential noise sources like power lines and houses were avoided. In addition, a number of soundings are aligned in two cross-sections, one of them overlapping both ERT profiles (See Fig. 4), which were conducted in March 2015.

The majority of the TEM soundings were conducted in the flat land, where sediments overlie the bedrock. In addition, two single TEM tests were conducted close to the bedrock outcrops to get the distinctive resistivity of those rocks. Figure 5 shows models corresponding to the

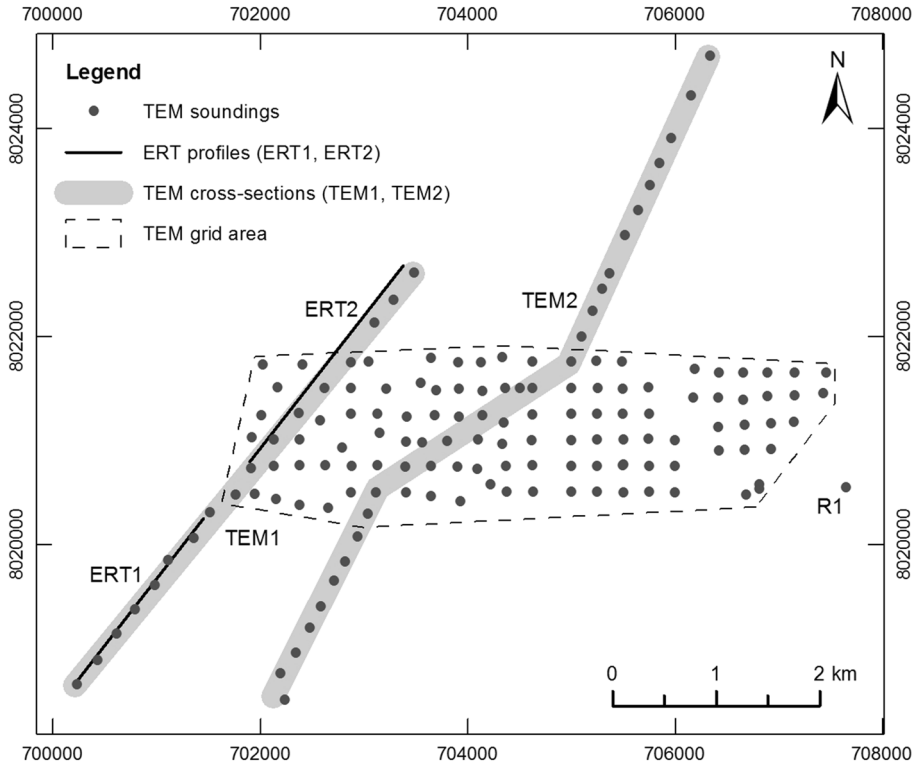

Fig. 4 Distribution of TEM and ERT measurements

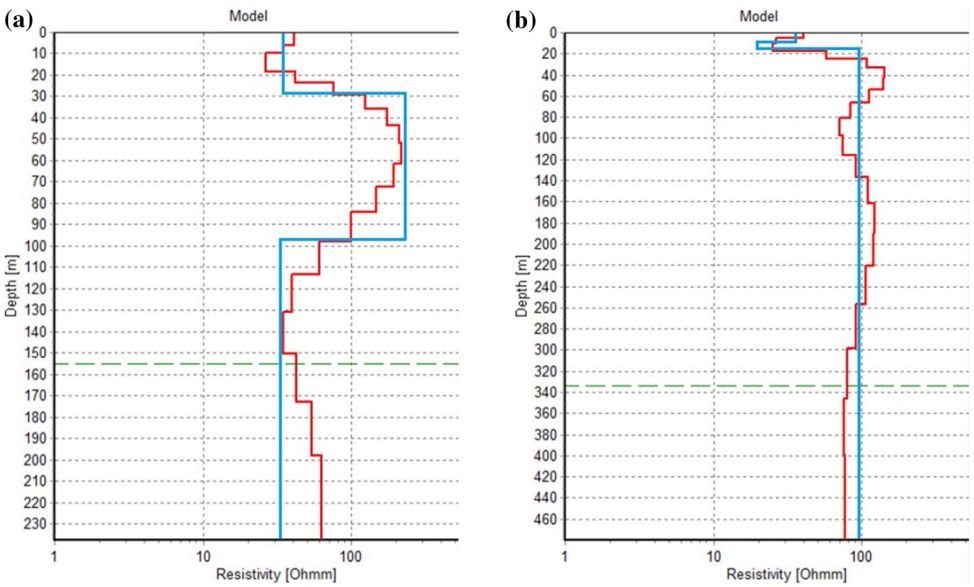

Fig. 5 TEM control soundings. Layered models in blue, smooth models in red. DOI in green dashed lines. **a** R1. Located close to the grid (see Fig. 4). **b** R2. Located up north of the study area (see Figs. 1, 2). R1 models show increasing resistivity below 29 m (bedrock); however, it decreases again below 97 m. However, it decreases to below 97 m. A more saline water flow or a different type of material at that level might be possible explanations. R2 models show a relatively constant high resistivity below 20 m

consolidated rock where values ≥ 100 Ω-m might be the characteristic of this type of geological unit.

The TEM soundings in the grid and nearby were similarly modeled by single one-dimensional inversions, which later were interpolated using the Kriging method to obtain horizontal resistivity maps and resistivity cross-sections. During the inversion process, a few soundings reached a DOI of 800 m which are assumed as outliers, while most of the soundings reached a depth between 100 and 400 m (see Fig. 6). Consequently, resistivity maps showed more blanks as they progress in depth (see Fig. 7).

A progressive resistivity visualization by depth is shown in Fig. 7. At the top slice, the map of resistivity distribution shows two distinctive parts; to the west, values about 30 Ω-m suggest dry sediments, although in the top 20 m from the surface, clay is more abundant, but the water content was small, because the tests were conducted from May to July (dry season). To the east, values between 5 and 10 Ω-m are in concordance with the presence of thermal springs and

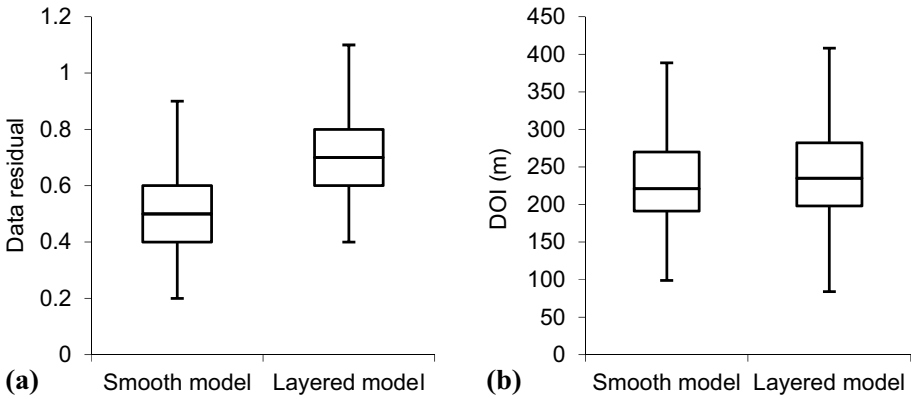

Fig. 6 Boxplots of **a** data residual and **b** DOI, for smooth and layered models corresponding to TEM data. Values in the boxplot represent the minimum, the first quantile, the median, the third quantile and the maximum. Soundings with data residual greater than 1 were removed. Most of the smooth models have smaller data residual than theirs correspondent layered models

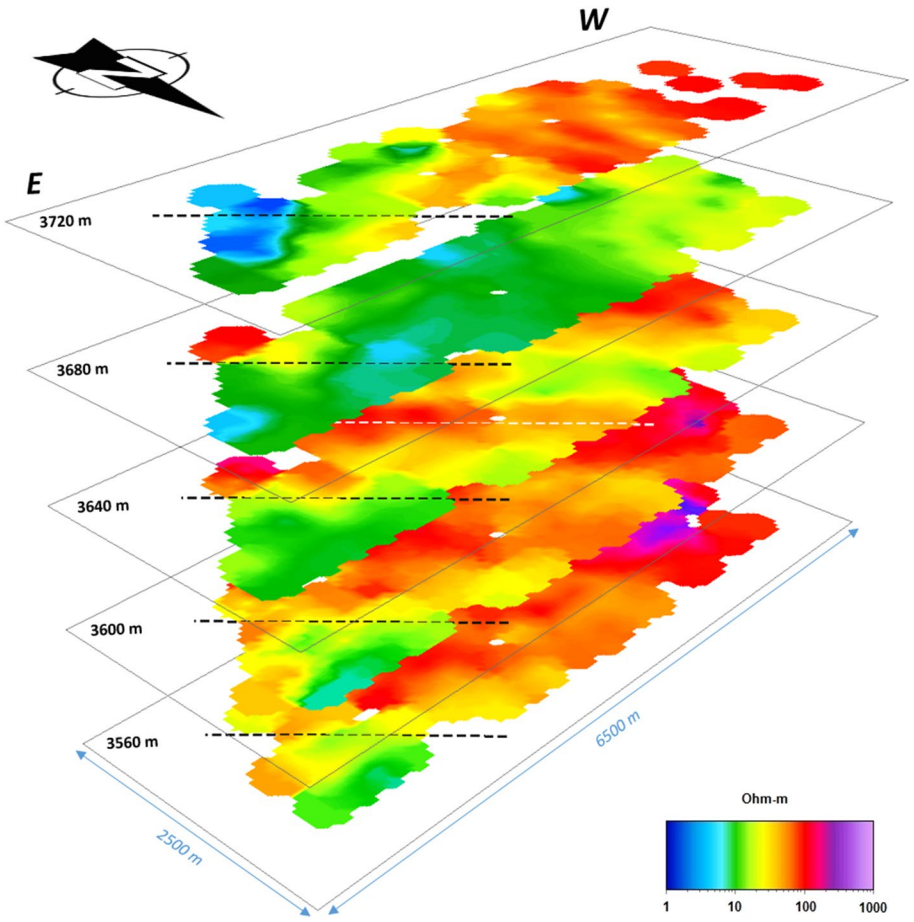

Fig. 7 Mean horizontal resistivity maps by depth (40 m separation), based on smooth models. Dashed lines marked in black indicate a trend of low values corresponding to the presence of saline water in a geological structure, and dashed line marked in white (slice 3640 m) indicate a bedrock fold, part of a complex bedrock relief

saline water disposed in this area. The next resistivity slice, at 3680 masl, is the most homogenous one, with values around 10 Ω-m, interpreted as fully saturated sediments. In addition, the most eastern part still exposes lower values linked with the hot springs. The next slice, at 3640 masl, starts showing higher values, which might indicate the relief of the bedrock exposing folds with southeast–northwest direction (white dashed line). For the rest of the slices below 3600 m, resistivity values remain almost constant, assumed as an indication of the DOI for most of the soundings not reaching these levels. Resistivity values ≥ 100 Ω-m in the western and central part of the grid, are characteristic of consolidated rock in this area. However, the most eastern part still shows lower values, suggesting in turn, the presence of ion-rich water. This trend is repeated in all the slices (black dashed line) which might be an indication of a geological structure, most likely a fault, where saline water is saturating the openings. Major faults in the region have the same direction, which lead to consider a possible connection.

The resistivity sections from the ERT tests are shown in Fig. 8. Profiles 1 and 2 (ERT1 and ERT2) show a thin surficial layer of a couple of meters with values around 80 Ω-m, this might indicate unsaturated sediments on top. Underlying the latter, lower values of around 20 Ω-m might indicate saturated sediments with a thickness varying from tens to hundreds of meters, following the relief of the bedrock. The bedrock has higher resistivity values ≥ 100 Ω-m. This interpretation is similar to those extracted from TEM results. However, ERT1 and ERT2 expose more detailed features, especially within the unconsolidated unit, because this technique generates a larger density of data for the tested profile in comparison to the TEM interpolations. For example, lenses of lower resistivity (~ 10 Ω-m), might indicate high clay content as it was seen in some pits in the area (Fig. 3).

The bedrock in ERT2 seems to sink into a depression to the northeast of the profile. To compare the resistivity distributions obtained from the ERT profiles, interpolations of TEM soundings are reported as cross-sections (TEM1 and TEM2). Figure 8 also shows two resistivity cross-sections based on smooth models and interpolated with the Kriging method, where it is possible to observe the uneven contact between basement rock and sediments. These cross-sections are perpendicular to the possible lengthening of some geological structures. The cross-section TEM1 overlaps the profiles ERT1 and ERT2 in the Fig. 8.

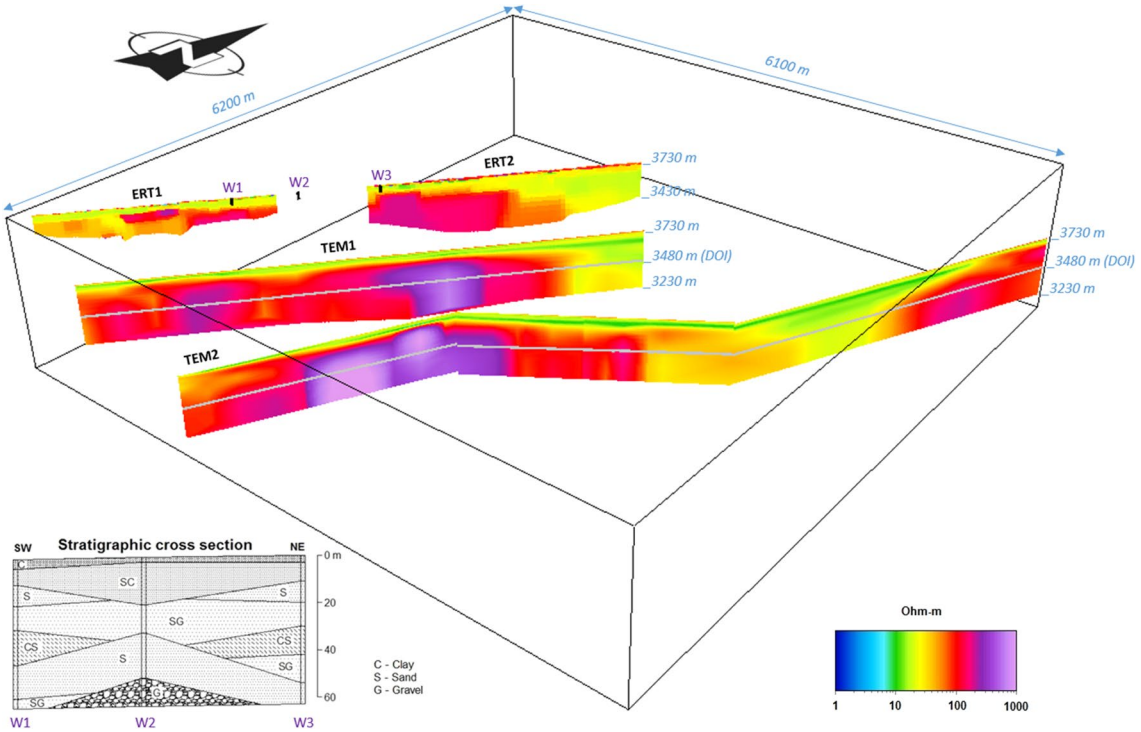

Fig. 8 3D image of resistivity sections from ERT and TEM. Profiles ERT1 and ERT2 are shown above TEM1 just for visualization purposes (ERT1, ERT2, TEM1 and wells W1, W2, W3 are located in the same line). ERT1 and ERT2 have different vertical resolution (DOI) because different electrode separations were used (10 and 20 m for ERT1 and ERT2, respectively). Stratigraphic cross-sections from drilling protocols describe the first 60 m corresponding to the unconsolidated sediments. The DOI for TEM1 and TEM2 is indicated as lines 250 m below the surface, although the resolution of both profiles reaches deeper levels because of the interpolation of the deepest soundings

The same resistive layer on top indicated in ERT1 and ERT2, is also shown in TEM1 and TEM2 as a thin layer. Values about 50 Ω-m might correspond to the surficial unsaturated sediments (as seen in Fig. 3). Just a few meters below the latter, the resistivity decreases to about 10 Ω-m, which might be an indication of saturated sediments. The thickness of these sediments varies according to the bedrock relief, from few meters to about 100 m. In the southwesternmost part of TEM2, the layer of saturated sediments is just a couple of meters, because the Silurian bedrock is outcropping nearby (see Fig. 2). Both TEM cross-sections show distinctive zones of high resistivity (≥ 500 Ω-m in purple), this feature might be an indication of consolidated bedrock with small to non-existent porosity and therefore low water storage. The big purple zones in TEM1 and TEM2 might correspond to the same structure, probably a buried ridge, which has similar direction (northwest–southeast) to the surficial outcrops, ridges and mountains in the region.

The settings and distribution of sediments (gravel, sand and clay) showed in the stratigraphic cross-section of Fig. 8 are difficult to distinguish just looking at the resistivity distribution in cross-sections ERT1, ERT2 and TEM1. The factors impeding a clear distinction might be the scale of the resistivity models and most important, the porosity and saturation degree of the sedimentary package, which makes the apparent resistivity being in the same range despite the difference in grain size distribution. Only the top clay layer differentiates itself from the rest of the unconsolidated materials due to its dryness.

Banks et al. (2002) reported the contact between sediments and bedrock located at 3580 masl in the northeast part of TEM1. In this cross-section, the resistivity corresponding to saturated sediments is still present even at 3300 m. Similarly, in a notorious part of TEM2, low resistivity might suggest the existence of deep valleys filled with sediments containing water. However, these hypothetical deep features do not coincide with the bedrock contour map (Banks et al. 2002), nor they do appear in the regional geological cross-section (Fig. 2b). The answer might be found in some structures and faults of the consolidated hard rock with southeast–northwest direction, which probably continue even below the unconsolidated sediments. Figure 9 shows the resistivity at 3650 m where the aligned distribution of low values coincides with the direction of two faults located to the southeast of the study area.

Discussion

The shallow resistivity to the east of the grid (Fig. 7a), about 5 Ω-m, is influenced by the high salinity of water coming out from the hot springs (EC ~ 3.6 mS/cm). A similar type of water might be present in the inferred faults (Fig. 9) and around them as well, playing a key role when it comes to determining the characteristic resistivity at different levels

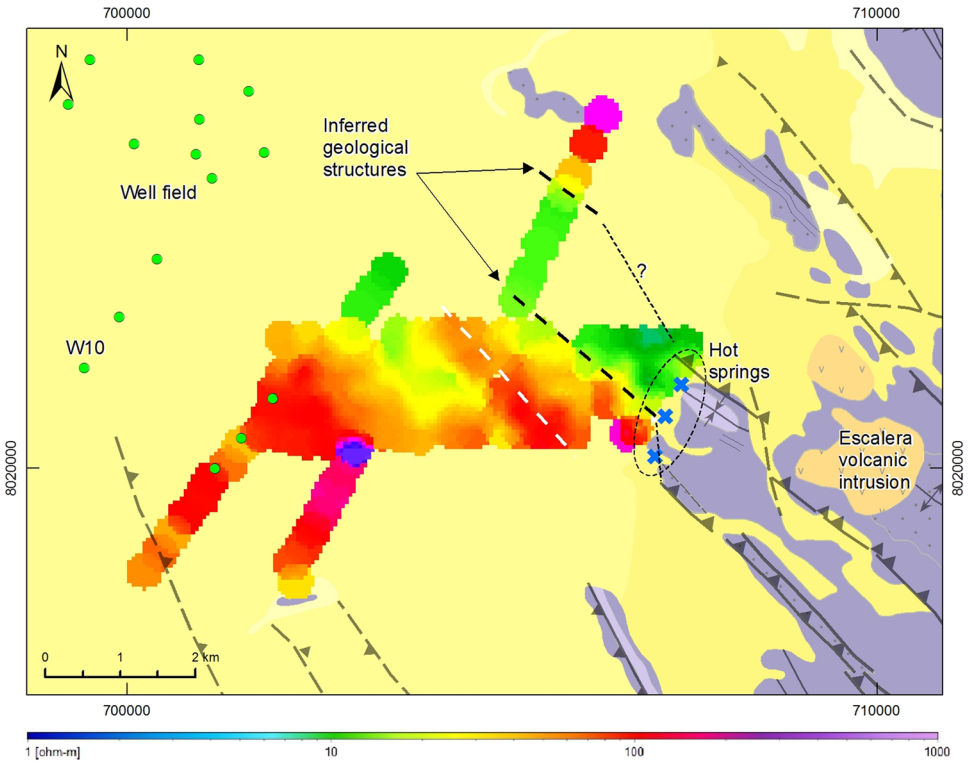

Fig. 9 Resistivity map at 3650 masl (about 70 mbs) from TEM soundings. Transparent geological map as the background (same as Fig. 2). The direction of the geological structures exposed in this map, from southeast to northwest, coincides with the alignment of the surficial ridges and faults indicated in the geological map. Hot springs are indicated with x close to the faults. Modified from GEOBOL and Swedish Geological (1992)

in the study area. The closeness of the Escalera volcanic intrusion might lead to think that this geological formation is contributing to the salinity enrichment and temperature rise of the groundwater especially in the faults. The process of dissolution and mixing of waters might happen further away from the limits of the investigation area or perhaps at greater depths. The geothermal sources in the region might be even more complex. An example of the last is the well W10 (Fig. 9), where the total penetration is 98 m, still within the porous aquifer. Its screen (from 65 to 85 mbs) seems to catch an ascending thermal flow, because the well presents artesian conditions and high salinity (3.5 mS/cm). Although the closest fault to W10 (left side in Fig. 9) does neither seem to be in contact with the Escalera volcanic intrusion nor with the Oruro complex, but an unknown geological formation indicated in Fig. 2b (brown color) might be the geothermal source.

The electromagnetic surveys in the study area aim to acquire characteristics of the subsurface at different depths expressed as resistivity; this feature is strongly influenced by the salinity of water stored in the voids. The average EC in the porous aquifer is 1.0 mS/cm (Gómez et al. 2016) and the resistivity of the unconsolidated and saturated sediments vary from 10 to 20 Ω-m, according to Fig. 7. In those parts where the groundwater is influenced by the geothermal activity, salinity increases (until 3.6 mS/cm) and therefore resistivity decreases (5 Ω-m) as it is observed around the hot springs (first slice of Fig. 7). The deeper the geophysical investigations reach, the lesser is the water content expected in the bedrock, as also indicated by the decreasing hydraulic conductivity with depth (Table 1). Low resistivity values of ~ 20 Ω-m are present at the bottom of the ERT2 profile and at the DOI mark of the cross-sections TEM1 and TEM2 (see Fig. 8), perhaps as indications of the presence of thermal and saline water in the inferred structures. The trend of the resistivity distribution coincides with the direction of faults projected below the study area.

Despite the influence of saline water, especially to the east of the TEM grid, the rest of the study area was surveyed consistently, distinguishing saturated alluvial sediments from the bedrock through their resistivity. The thickness of the sediments varies from a couple of meters (to the north and south ends of the TEM2 in Fig. 8) to about 80 m in the centre of the grid. Low resistivity values are found at deeper levels as well, however, they might be associated with the influence of saline water, as it was explained before. The slope of the bedrock, indicated by Banks et al. (2002), as an even depression from east to west in the grid area (see Fig. 2), seems to be more complex since there are indications of buried folds appearing at 40–80 mbs (see Fig. 10). These folds have the same direction as the rest of the structures in the subsoil, from southeast to northwest. Therefore, a detailed resolution of the bedrock relief was achieved with the geo-electrical methods used in this study. These methods can be used extensively to improve the understanding of the thickness of the sediments in the rest of the aquifer system.

Conclusions

Geophysical investigations applying transient electromagnetic soundings (TEM) and electrical resistivity tomography (ERT) methods in the area of the Challapampa aquifer system, made it possible to generate new information exposing geological structures like faults and buried folds, which were not previously identified. The findings of this study might

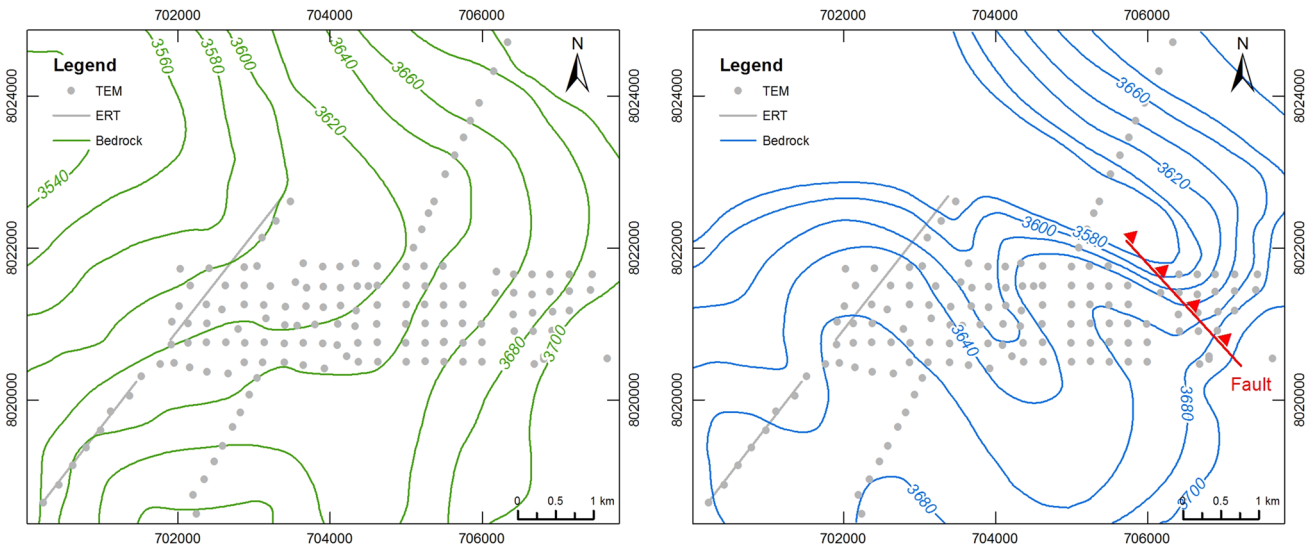

Fig. 10 Contour bedrock map from previous studies (Banks et al. 2002) to the left and inferred from geo-electrical methods to the right

help to improve the understanding of the hydrogeological characteristics of the aquifers in the region.

The ERT and TEM results complemented each other very well. Unconsolidated sediments, both dry and saturated, and consolidated rock have distinctive resistivity signatures, low values for the alluvium and high values for the bedrock. Although TEM investigations are recommended at sites where more conductive deep formations limit the DOI, some places with more resistive formations at lower limits were successfully interpreted with TEM methods like in the present study. In the study area, the typical resistivity values for the consolidated rock in the nearby outcrops are similar to those corresponding to the bedrock at about 80 mbs, under the unconsolidated sediments, in the grid area and in the resistivity cross-sections. However, the contact between sediments and hard rock looks irregular and complex, more than how it is shown in the bedrock contour lines in Fig. 2a from previous studies, maybe because similar geological processes might have shaped the superficial mountainous landscape and the buried bedrock.

The characteristics of water, especially the salinity, determine the resultant resistivity of the ground. The distribution of resistivity, at depths coinciding with the contact between the unconsolidated sediments and the bedrock, seems aligned with the trend of faults indicated in the geological map. These results suggest the existence of faults and other geological structures under the sediments, probably as lengthening of other structures to the southeast of the study area. The geological structures, like faults and folds, newly inferred and previously reported have a similar direction from southeast to northwest.

The two types of water influencing the resistivity images in the study area, fresh water in the unconsolidated sediments and more saline water close to some faults and structures in the bedrock, suggest the distinction of two different aquifers; a porous aquifer in the sediments on top (from the surface until the contact with the bedrock) and a fractured aquifer in the consolidated bedrock underlying the latter.

A more detailed resolution of the shape of the bedrock, and therefore the thickness of the alluvial sediments was evaluated in the study area. The thickness of the alluvial aquifer ranges from a couple of meters to about 120 m. These results improve the understanding of the geometry of the aquifer system. More extended investigations of this type are required to estimate the thickness of the porous aquifer in the rest of the reservoir, a parameter required in turn to evaluate the aquifer storage.

Acknowledgements The study was funded by the Swedish International Development Cooperation Agency (SIDA) and the Society of Exploration Geophysicists (SEG) through the Geoscientists Without Borders (GWB) programme. This work was also supported by Lund University (LU) in Sweden, Aarhus University (AU) in Denmark, and Universidad Mayor de San Andrés (UMSA) and Universidad Técnica de Oruro (UTO) in Bolivia. The TEM equipment was provided by Engineering Geology Division of Lund University with support from Guideline Geo AB. The ERT equipment was provided by UTO and Unidad de Saneamiento Básico y Vivienda (UNASVBI). We are grateful to Rafael Mendoza for helping in the field work, personnel of Corimex Ltda. for joining in field work for a couple of days. Conny Svensson from Engineering Geology, LU, for a thorough revision of the manuscript and also Esben Auken, Nikolaj Foged and other personnel of Hydrogeophysics Group Department of Geoscience, AU, for providing TEM setups, advice and support.

Open Access This article is distributed under the terms of the Creative Commons Attribution 4.0 International License (http://creativecommons.org/licenses/by/4.0/), which permits unrestricted use, distribution, and reproduction in any medium, provided you give appropriate credit to the original author(s) and the source, provide a link to the Creative Commons license, and indicate if changes were made.

References

Aarhus GeoSoftware (2017a) Aarhus SPIA, Aarhus. 8000 Aarhus C, Denmark

Aarhus GeoSoftware (2017b) Aarhus Workbench, Aarhus. 8000 Aarhus C, Denmark

Auken E, Jørgensen F, Sørensen KI (2003) Large-scale TEM investigation for groundwater. Explor Geophys 34:188. https://doi.org/10.1071/EG03188

Banks D, Holden W, Aguilar E, Mendez C, Koller D, Andia Z, Rodriguez J, Saether OM, Torrico A, Veneros R, Flores J (2002) Contaminant source characterization of the San Jose Mine, Oruro, Bolivia. Geol Soc Lond Special Publ 198:215–239. https://doi.org/10.1144/GSL.SP.2002.198.01.14

Boiero D, Godio A, Naldi M, Yigit E (2010) Geophysical investigation of a mineral groundwater resource in Turkey. Hydrogeol J 18:1219–1233. https://doi.org/10.1007/s10040-010-0604-2

Christiansen AV, Auken E (2012) A global measure for depth of investigation. Geophysics 77:WB171–WB177. https://doi.org/10.1190/geo2011-0393.1

Christiansen AV, Auken E, Sørensen K (2009) The transient electromagnetic method. In: Kirsch R (ed) Groundwater geophysics: a tool for hydrogeology. Springer, Berlin, pp 179–226

Corriols M, Nielsen MR, Dahlin T, Christensen NB (2009) Aquifer investigations in the Leon-Chinandega plains, Nicaragua, using electromagnetic and electrical methods. Near Surf Geophys 7:413–425. https://doi.org/10.3997/1873-0604.2009034

Dahlin T (2001) The development of DC resistivity imaging techniques. Comput Geosci 27:1019–1029. https://doi.org/10.1016/S0098-3004(00)00160-6

Dahlin T, Zhou B (2006) Multiple-gradient array measurements for multichannel 2D resistivity imaging. Near Surf Geophys 4:113–123. https://doi.org/10.3997/1873-0604.2005037

Dames & Moore Norge (2000) Estudio hidrogeológico de la mina San José y los acuíferos que suministran agua a la ciudad de Oruro (Hydrogeological Study of the San Jose Mine and Adjacent Aquifers Supplying Water to the City of Oruro): Report 1,2,3., PMAIM-Subproyecto No 7. Corporacion Minera de Bolivia COMIBOL, Oruro, Bolivia, p 229

GEOBOL, Swedish Geological AB (1992) Carta Geológica de Bolivia - Hoja Oruro (Geological map of Bolivia - Sheet Oruro). Publicación SGB Serie I-CGB-11, p 6140

GITEC CG, COBODES L (2014) Formulación del Plan Director de la cuenca del lago Poopó (Poopo Lake Basin Management Plan

Formulation). Informe final. Programa de gestion sostenible de los recursos naturales de la cuenca del lago Poopo. Gobierno Autonomo Departamental de Oruro. Agosto 2014, Oruro, Bolivia (CTO-SERV-03/2013), p 561

Gómez E, Barmen G, Rosberg J-E (2016) Groundwater origins and circulation patterns based on isotopes in Challapampa aquifer. Bolivia Water 8:207. https://doi.org/10.3390/w8050207

Gonzales A, Dahlin T, Barmen G, Rosberg J-E (2016) Electrical resistivity tomography and induced polarization for mapping the subsurface of alluvial fans: a case study in Punata (Bolivia). Geosciences 6:51. https://doi.org/10.3390/geosciences6040051

Guérin R, Descloitres M, Coudrain A, Talbi A, Gallaire R (2001) Geophysical surveys for identifying saline groundwater in the semi-arid region of the central Altiplano, Bolivia. Hydrol Process 15:3287–3301. https://doi.org/10.1002/hyp.284

Larsson M (2016) TEM investigation on Challapampa aquifer, Oruro Bolivia. Geology Department, Lund University, MSc Thesis No 494, p 47

Lizarazu J, Aranyossy JF, Orsag V, Salazar JC (1987) Estudio Isotopico de la cuenca de Oruro-Caracollo, Bolivia (Isotopic study in the Oruro-Caracollo basin, Bolivia). Isotope techniques in water resources development IAEA-SM-299/11 301-314, Vienna, Symposium March 1987

Loke MH, Acworth I, Dahlin T (2003) A comparison of smooth and blocky inversion methods in 2D electrical imaging surveys. Explor Geophys 34:182–187

Metwaly M, El-Qady G, Massoud U, El-Kenawy A, Matsushima J, Al-Arifi N (2010) Integrated geoelectrical survey for groundwater and shallow subsurface evaluation: case study at Siliyin spring, El-Fayoum, Egypt. Int J Earth Sci 99:1427–1436. https://doi.org/10.1007/s00531-009-0458-9

Nabighian M (1991) Electromagnetic methods in applied geophysics: Volume 2, Application, Parts A and B. Newmont Exploration Limited ed. Society of Exploration Geophysicists, Denver, Colorado, US. https://doi.org/10.1190/1.9781560802686

Patureau N (2007) Contamination of the groundwater in Oruro city (Bolivia) and possible solutions to avoid polluting more in the future. MSc Thesis. No 069116458, School of Civil Engineering and Geosciences. Newcastle University, p 119

Ramos OE, Caceres LF, Ormachea MR, Bhattacharya P, Quino I, Quintanilla J, Sracek O, Thunvik R, Bundschuh J, Garcia ME (2011) Sources and behavior of arsenic and trace elements in groundwater and surface water in the Poopó Lake Basin, Bolivian Altiplano. Environ Earth Sci 66:793–807. https://doi.org/10.1007/s12665-011-1288-1

Reynolds JM (2011) An introduction to applied and environmental geophysics. Wiley, New York

Rigsby CA, Bradbury JP, Baker PA, Rollins SM, Warren MR (2005) Late Quaternary palaeolakes, rivers, and wetlands on the Bolivian Altiplano and their palaeoclimatic implications. J Quat Sci 20:671–691. https://doi.org/10.1002/jqs.986

SCIDE, CORDEOR, GEOBOL (1996) Informe de los pozos de producción - Proyecto de investigación y verificación de fuentes de abastecimiento de agua para la ciudad de Oruro (Report of the production wells - Project of investigation and verification of sources of water for supplying Oruro). GEOBOL - Servicio Geológico de Bolivia, Oruro, p 159

SELA (2017) Servicio Local De Acueductos Y Alcantarillado—Oruro. http://selaoruro.gob.bo/ Accessed 01 Jul 2017

SENAMHI (2015) Servicio Nacional de Meteorologia e Hidrologia de Bolivia. http://senamhi.gob.bo/. Accessed 9 Apr 2015

Spies BR (1989) Depth of investigation in electromagnetic sounding methods. Geophysics 54:872–888. https://doi.org/10.1190/1.1442716

Suarez Soruco R (2000) Compendio de Geología de Bolivia (Bolivian Geology Compendium), vol 18. Revista técnica de Yacimientos Petrolíferos Fiscales Bolivianos, Cochabamba, Bolivia, pp 213

Swedish Geological AB (1996) Impacto de la contaminación minera e industrial sobre agua subterráneas (Impact of mining and industrial pollution on groundwater). Ministerio de Desarrollo Sostenible y Medio Ambiente. Secretaria Nacional de Mineria. Proyecto Poloto Oruro. ID: R-Bo-E-9.45-9702-PPO96I6, Oruro, Bolivia, p 117

Publisher's Note Springer Nature remains neutral with regard to jurisdictional claims in published maps and institutional affiliations.